Inorganic Chemistry

Article

pubs.acs.org/IC

Magnetic Sponge Phenomena Associated with Interchain Dipole–Dipole Interactions in a Series of Ferrimagnetic Chain Compounds Doped with Minor Diamagnetic Species

Masaki Nishio[†] and Hitoshi Miyasaka*[,‡]

[†]Department of Chemistry, Division of Material Sciences, Graduate School of Natural Science and Technology, Kanazawa University, Kakuma-machi, Kanazawa 920-1192, Japan

[‡]Institute for Materials Research, Tohoku University, 2-1-1 Katahira, Aoba-ku, Sendai 980-8577, Japan

Supporting Information

ABSTRACT: The donor/acceptor ionic chain (i.e., the D^+A^- chain) $[Ru_2(2\text{-MeO-4-ClPhCO}_2)_4(BTDA\text{-}TCNQ)]\cdot 2.5(benzene)$ (**1**; 2-MeO-4-$ClPhCO_2^-$ = 2-methoxy-4-chlorobenzoate; BTDA-TCNQ = bis(1,2,5-thiadiazolo)tetracyanoquinodimethane) is a ferrimagnetic chain with S = 3/2 from $[Ru_2^{II,III}]^+$ (i.e., D^+) and S = 1/2 from $BTDA\text{-}TCNQ^{\bullet-}$ (i.e., A^-), with $J \approx -100$ K, in which long-range antiferromagnetic ordering at T_N = 11 K occurs because interchain antiferromagnetic interactions are critical. Compound **1** undergoes a reversible crystal-to-crystal structural transformation with the elimination/absorption of the crystallization solvent to form the dried compound $[Ru_2(2\text{-MeO-4-ClPhCO}_2)_4(BTDA\text{-}TCNQ)]$ (**1′**), which has a higher T_N (14 K). This change is clearly caused by the shortening of the interchain distances because the exchange coupling parameter for the chain is the same in both **1** and **1′**. The chain compounds in **1** can be doped with minor diamagnetic $[Rh_2^{II,II}]$ species, $[\{(Ru_2)_{1-x}(Rh_2)_x(2\text{-MeO-4-ClPhCO}_2)_4\}(BTDA\text{-}TCNQ)]\cdot 2.5(benzene)$ (x = 0.03 for **Rh-3%**; x = 0.05 for **Rh-5%**; x = 0.16 for **Rh-16%**), which shifts the T_N to lower temperatures, the magnitude of the shift being dependent on the doping ratio x (T_N = 5.9 K for **Rh-3%**, T_N = 3.7 K for **Rh-5%**, and T_N was not observed above 1.8 K for **Rh-16%**). Drying a doped compound increased its T_N, as was found for **1′**: T_N = 9.9 K for **Rh-3%′**, T_N = 9.2 K for **Rh-5%′**, and T_N was not observed above 1.8 K for **Rh-16%′**. T_N had a linear relationship with the doping ratio x of the $[Rh_2]$ species in both the fresh and dried compounds. The T_N linear relationship is associated with the magnitude of the effective magnetic dipole (i.e., the average correlation length) in the chains caused by the $[Rh_2]$ defects as well as naturally generated defects in the synthetic process and with the interchain distances affected by the crystal-to-crystal transformations. These results demonstrate that slightly modifying the short-range correlation lengths, which changes the magnetic dipole magnitudes, strongly affects the bulk antiferromagnetic transition, with key dipole–dipole interactions, in low-dimensional anisotropic systems.

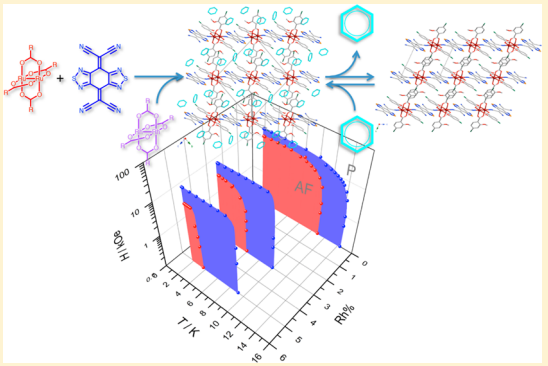

INTRODUCTION

Electron donor (D)/electron acceptor (A) charge transfer (CT) systems are potentially good magnetic materials.[1] This is because such a system has two properties that are very useful in producing high-efficiency magnetic materials: (1) its spin state switches between two critical states, neutral (N) and ionic (I), involving electron transfer (ET),[2] and (2) the ionic state, with a newly produced spin set, often allows a relatively strong spin correlation $|J|$, sometimes of over 100 K, supported by CT between ionized D^+ and A^- units. Using transition metal complexes that have ionic states with high spin multiplicities (i.e., classical spins) as D and A building blocks are preferred in the synthesis of such ET magnetic materials because the I state with one electron transfer (i.e., D^+A^-) can always have an effective magnetic moment, even with antiferromagnetic coupling between spin sets. A good example of such a strategy can be seen in the ferrimagnetic series of Mn^{III} porphyrin (S = 2)/organic anionic radical (S = 1/2) designed by Miller et al., in which a Mn^{II} porphyrin and an organic acceptor are assembled, accompanied by ET.[3−8] We have focused on a D/A combination of a paddlewheel-type diruthenium(II, II) complex (abbreviated hereafter as $[Ru_2^{II,II}]$) and an organic polycyano acceptor such as 7,7,8,8-tetracyano-*p*-quinodimethane (TCNQ) or *N*,*N*′-dicyanoquinonediimine (DCNQI).[9] The $[Ru_2^{II,II}]$ is a donor with an S = 1 spin state, which is changed to an S = 3/2 state in the one-electron ($1e^-$) oxidized $[Ru_2^{II,III}]^+$ species.[10] The diamagnetic organic polycyano acceptor has an S = 1/2 state in its $1e^-$ reduced form, $TCNQ^{\bullet-}$ or $DCNQI^{\bullet-}$. This D/A combination has allowed the construction of multidimensional frameworks called D/A–metal–organic frameworks (i.e., D/A–MOFs) that involve CT/ET and has

Received: February 20, 2014
Published: April 21, 2014

allowed the production of good magnetic materials with high Curie or Néel temperatures (reaching 100 K in several cases with $1e^-$ transferred two- and three-dimensional network D_2A materials).[11]

Recently, our group successfully isolated a stable ionic D^+A^- chain compound in the $[Ru_2]$/TCNQ series, $[Ru_2(2\text{-MeO-4-ClPhCO}_2)_4(BTDA\text{-}TCNQ)]\cdot 2.5(benzene)$ (**1**; 2-MeO-4-$ClPhCO_2^-$ = 2-methoxy-4-chlorobenzoate; BTDA-TCNQ = bis(1,2,5-thiadiazolo)tetracyanoquinodimethane), which was the first example of an ionic D^+A^- chain compound in the $[Ru_2]$/TCNQ series obtained at ambient temperatures. Its ET-inert/diamagnetic $[Rh_2^{II,II}]$-doped product, with the formula $[\{(Ru_2)_{1-x}(Rh_2)_x(2\text{-MeO-4-ClPhCO}_2)_4\}(BTDA\text{-}TCNQ)]\cdot 2.5(benzene)$ (x = 0.03 for **Rh-3%**; x = 0.05 for **Rh-5%**; x = 0.16 for **Rh-16%**), exhibited unique electronic conduction that was dependent on the amount of dopant present.[12] Here, we will focus on the magnetic properties of these newly synthesized isostructural chain compounds and their solvent-free forms (the dried compounds **1′**, **Rh-3%′**, **Rh-5%′**, and **Rh-16%′**) (Scheme 1). Compound **1** has ferrimagnetic spin short-range ordering

Scheme 1

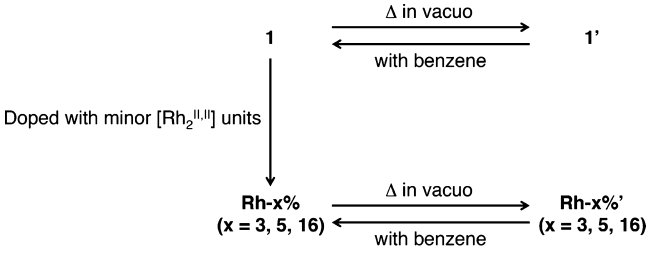

with S = 3/2 and S = 1/2 and strong intrachain antiferromagnetic coupling with $J \approx -100$ K, followed by long-range antiferromagnetic ordering at $T_N \approx 11$ K caused by the effects of interchain antiferromagnetic interactions. In addition, **1** undergoes a reversible crystal-to-crystal transformation when it is dried at 50 °C *in vacuo*, giving a stable new crystal phase, **1′**, with $T_N \approx 14$ K; **1′** has a modified interchain environment and easily returns to the original **1** form when it absorbs benzene molecules at room temperature. These types of material were called "magnetic sponges"[11g,13] (Scheme 1). Interestingly, in addition to the crystal-to-crystal transformation, doping **1** with $[Rh_2^{II,II}]$ instead of $[Ru_2^{II,II}]$ systematically modifies T_N, despite the fact that no significant structural differences exist between the original compound (**1** or **1′**) and the corresponding doped compound. In this Article, we report the precise tuning of the magnetic phase in this series of chain compounds by combining two chemical techniques: (i) desolvation/solvation of the crystal phase and (ii) doping with diamagnetic species. Both techniques are associated with changes in interchain dipole−dipole interactions.

EXPERIMENTAL SECTION

Materials. The solvated compounds **1**, **Rh-3%**, **Rh-5%**, and **Rh-16%**, and the all-Rh derivative of **1**, $[Rh_2(2\text{-MeO-4-ClPhCO}_2)_4(BTDA\text{-}TCNQ)]\cdot 2.5(benzene)$ (**2**), were prepared following the published method.[12] All of the synthetic procedures were performed under N_2 atmosphere using standard Schlenk techniques and a commercial glovebox. Dry samples were prepared by heating the fresh samples (**1**, **Rh-3%**, **Rh-5%**, **Rh-16%**, and **2**) *in vacuo* for 17 h at 50 °C. For **1′**, elemental analysis (%) calcd for $C_{44}H_{24}Cl_4N_8O_{12}Ru_2S_2$, C 41.78, H 1.91, N 8.86; found, C 42.03, H 2.22, N 8.66. FT-IR (KBr; cm^{-1}): ν(C≡N) 2189, 2171; ν(C═O) 1596, 1406, 1381. For **2′**, elemental analysis (%) calcd for $C_{44}H_{24}Cl_4N_8O_{12}Rh_2S_2$, C 41.78, H 1.91, N 8.86; found, C 41.61, H 2.05, N 8.65. FT-IR (KBr; cm^{-1}): ν(C≡N) 2236, 2218; ν(C═O) 1600, 1406, 1377. For **Rh-3%′**, elemental analysis (%) calcd for $C_{44}H_{24}Cl_4N_8O_{12}Rh_{0.06}Ru_{1.94}S_2$, C 41.78, H 1.91, N 8.86; found, C 42.03, H 2.27, N 8.49. FT-IR (KBr; cm^{-1}): ν(C≡N) 2190, 2170; ν(C═O) 1596, 1405, 1381. For **Rh-5%′**, elemental analysis (%) calcd for $C_{44}H_{24}Cl_4N_8O_{12}Rh_{0.1}Ru_{1.9}S_2$, C 41.78, H 1.91, N 8.86; found, C 41.76, H 2.27, N 9.18. FT-IR (KBr; cm^{-1}): ν(C≡N) 2190, 2167; ν(C═O) 1596, 1405, 1381. For **Rh-16%′**, elemental analysis (%) calcd for $C_{44}H_{24}Cl_4N_8O_{12}Rh_{0.32}Ru_{1.68}S_2$, C 41.76, H 1.91, N 8.86; found, C 42.06, H 2.11, N 9.21. FT-IR (KBr; cm^{-1}): ν(C≡N) 2190, 2168; ν(C═O) 1595, 1406, 1380.

Identification and Physical Measurements. Infrared spectra were measured, using a KBr disk, with a HORIBA FT-720 or a JASCO FT/IR-4200 spectrophotometer. Thermogravimetric analysis was performed using a Shimadzu DTG-60H instrument under a flowing N_2 atmosphere, and the temperature was increased from room temperature to 400 °C at a rate of 5 °C/min. DSC data were collected over the temperature range 25−180 °C and increased or decreased at a rate of 2 °C min^{-1}, using a Shimadzu DSC-60 instrument. Magnetic susceptibility measurements were performed using a Quantum Design SQUID magnetometer (MPMS-XL). DC measurements were performed over the temperature range 1.8−300 K and from −7 to +7 T. AC measurements were performed at 1 Hz with an AC field amplitude of 3 Oe in the absence of a DC field. The measurements were performed on finely ground polycrystalline samples mixed with Nujol. Diamagnetic contributions were corrected for the sample holder, the Nujol, and the sample using Pascal's constants.[14]

X-ray Crystallography of 1′. Single crystals of **1′** were prepared following the method described in the synthetic procedure. A single crystal with a size of 0.107 × 0.031 × 0.029 mm^3 was mounted with Nujol on a thin kapton film and cooled to 97 ± 1 K with a stream of cooled N_2. Data were collected using a Rigaku CCD diffractometer (Mercury70 + varimax) with graphite-monochromated MoKα radiation (λ = 0.71070 Å). A full-matrix least-squares refinement on F^2 was performed, based on the observed reflections and variable parameters, and the refinement cycle was estimated from the unweighted agreement factor $R_1 = \Sigma||F_o| - |F_c||/\Sigma|F_o|$ ($I > 2.00\sigma(I)$ and all data) and the weighted agreement factor $wR_2 = [\Sigma(w(F_o^2 - F_c^2)^2)/\Sigma w(F_o^2)^2]^{1/2}$ (all data). A Sheldrick weighting scheme was used. Neutral atom scattering factors published by Cromer and Waber were used.[15] Anomalous dispersion effects were included in F_{calcd},[16] and the $\Delta f'$ and $\Delta f''$ values published by Creagh and McAuley were used.[17] The mass attenuation coefficient values published by Creagh and Hubbell were used.[18] The calculations were performed using the CrystalStructure crystallographic software package,[19] except for the refinement process, which was performed using SHELXL-97.[20] The CIF data for **1′** were deposited at the Cambridge Crystallographic Data Centre (CCDC) in supplementary publication No. CCDC-895010. Copies of the data can be obtained free of charge from CCDC, 12 Union Road, Cambridge CB2 1EZ, UK (fax, +44 1223 336 033; e-mail, deposit@ccdc.cam.ac.uk).

Crystallographic Data for 1′. $C_{44}H_{24}Cl_4N_8O_{12}Ru_2S_2$, M_r = 1264.79, triclinic, $P\bar{1}$ (#2), a = 10.544(11) Å, b = 10.858(9) Å, c = 11.739(10) Å, α = 114.00(3)°, β = 94.84(5)°, γ = 93.09(5) °, V = 1218(2) $Å^3$, T = 97(1) K, Z = 1, D_{calc} = 1.725 g cm^{-3}, F_{000} = 628, λ = 0.71075 Å, μ(Mo Kα) = 9.954 cm^{-1}, 7944 measured reflections, 4180 unique reflections (R_{int} = 0.0342), R_1 = 0.0724 ($I > 2\sigma(I)$), R_1 = 0.0955 (all data), and wR_2 = 0.1907 (all data) with GOF = 1.074. CCDC−895010.

X-ray Powder Diffraction of Rh-3%′, Rh-5%′, Rh-16%′, and 2′, and of the Conversion from 1′ to 1. X-ray powder diffraction (XRPD) spectra of the solvent-free dried samples were obtained using a Rigaku Ultima-IV diffractometer, CuKα radiation (λ = 1.5418 Å), and at room temperature. A microcrystalline powder sample was put into a 0.5 mm diameter glass capillary and rotated. XRPD spectra were measured in the 2θ range 5−40°, with 0.02° steps. The crystal-to-crystal conversion of **1′** to **1** in benzene atmosphere was confirmed by performing XRPD measurements in the 2θ range 5−25°, with 0.05° steps (1 h per scan). After measuring **1′**, the capillary was kept under

dx.doi.org/10.1021/ic500413j | Inorg. Chem. 2014, 53, 4716−4723

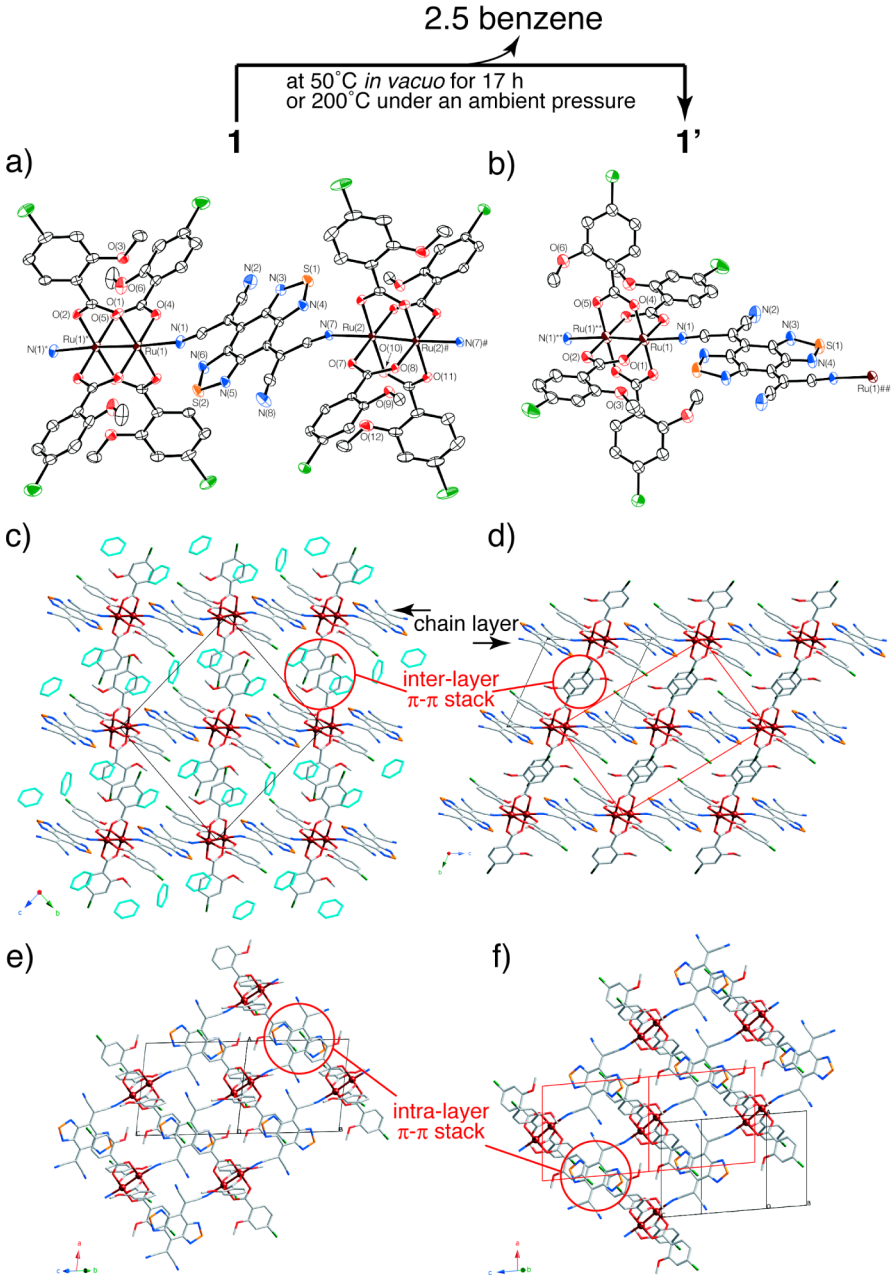

Figure 1. Crystal structures of **1** (a, c, and e) and **1′** (b, d, and f). (a and b) Ortep drawings of the asymmetric unit (50% probability ellipsoids; symmetry operation *, $-x-1, -y+1, -z+1$; #, $-x+1, -y+2, -z$; **, $-x, -y, -z+1$; ##, $-x+1, -y, -z$). (c and d) Packing diagrams projected along the *a* axis. The benzene molecules, as interstitial solvents in **1**, are shown in pale blue in c. (e and f) Packing of chains in the "chain layer" in the (011) plane. The red circles indicate the $\pi-\pi$ stacking parts, and the modified unit cell for **1′** is shown in red in d and f. Hydrogen atoms are omitted for clarity.

benzene and N_2 atmosphere for 10 min in a Schlenk tube, and the XRPD spectra of the benzene-exposed sample were then measured. This treatment was repeated until the XRPD pattern of **1′** was disappeared (approximately 1 h).

RESULTS AND DISCUSSION

Solvated Materials. Compounds **1** and **2** (the $[Rh_2^{II,II}]$ derivative of **1**) and the $[Rh_2^{II,II}]$-doped compounds $[\{(Ru_2)_{1-x}(Rh_2)_x(2\text{-MeO-4-ClPhCO}_2)_4\}(BTDA\text{-}TCNQ)]\cdot 2.5(benzene)$ ($x = 0.03$ for **Rh-3%**, $x = 0.05$ for **Rh-5%**, and $x = 0.16$ for **Rh-16%**) are isostructural and crystallize in the triclinic $P\bar{1}$ space group with $Z = 2$ (Figure 1a).[12] The structures of these compounds have already been described;[12] therefore, only the important frameworks needed for comparing them with the desolvated materials (vide infra) will be described here. The BTDA-TCNQ moiety in **1** acted as a linear-type bidentate ligand, using only two cyano groups in trans positions,[11d,e,h] forming a D^+A^- alternating chain that was similar to the chain compounds based on DCNQI.[2,21] There were two kinds of $[Ru_2]$ moieties in the asymmetric unit, and each had an inversion center at the midpoint of the Ru–Ru bond; therefore, the repeating unit can be described as half of $[-\{Ru(1)_2\}-(BTDA\text{-}TCNQ)-\{Ru(2)_2\}-(BTDA\text{-}TCNQ)-]$ (Figure 1a). The structures of both $[Ru_2]$ units and the bonded forms were very similar, and the oxidation state was assigned as $[Ru_2^{II,III}]^+$

dx.doi.org/10.1021/ic500413j | Inorg. Chem. 2014, 53, 4716–4723

for both units, whereas the BTDA-TCNQ moiety was BTDA-TCNQ$^{\bullet-}$.[12]

The chains ran in the ⟨21−1⟩ direction; therefore, on the (011) plane, they formed a chain-aggregated layer (later called a "chain layer"; see Figure 1c−f). The chains in this chain layer were closely packed in an antiphase manner, with interchain $\pi-\pi$ stacks between the 2-MeO-4-Cl-Ph group of $[Ru_2]$ and the BTDA-TCNQ, with least-squares plane-to-plane distances ($d_{LS\text{-}p-p}$) of 3.325 and 3.391 Å for $[Ru(1)_2]$ and $[Ru(2)_2]$, respectively. Consequently, the interchain distance was relatively short: the $[Ru_2]$···BTDA-TCNQ distances being 7.184(2) and 7.297(2) Å for $[Ru(1)_2]$ and $[Ru(2)_2]$, respectively, and the $[Ru(1)_2]$···$[Ru(2)_2]$ distance and the distance between BTDA-TCNQs being 10.479(2) Å (Figure S1, Supporting Information). The crystallization solvent molecules (2.5 benzene molecules per unit) were present between the chain layers (Figure 1c); therefore, the chains, which were aligned in-phase in the ⟨011⟩ direction, were significantly separated with a distance of 11.849(3) Å between BTDA-TCNQs and a $[Ru(1)_2]$···$[Ru(2)_2]$ distance of 12.467(2) Å (Figure S1, Supporting Information). There was a $\pi-\pi$ stacking form between benzoate groups, with $d_{LS\text{-}p-p}$ = 3.409 Å (Figure 1c) and a minimum C···C distance of 3.587(5) Å.

Crystal-to-Crystal Transformation by Eliminating/Inserting Crystallization Solvent Molecules. Each of the solvated compounds **1**, **Rh-3%**, **Rh-5%**, **Rh-16%**, and **2** underwent a crystal-to-crystal transformation to form the corresponding dried sample (**1′**, **Rh-3%′**, **Rh-5%′**, **Rh-16%′**, and **2′**) through the elimination of the crystallization solvent (2.5 benzene molecules per unit) at ca. 100 °C at ambient pressure (the decomposition temperature was ca. 230 °C) (Figure S2, Supporting Information, for **1**). Figure 2 shows the

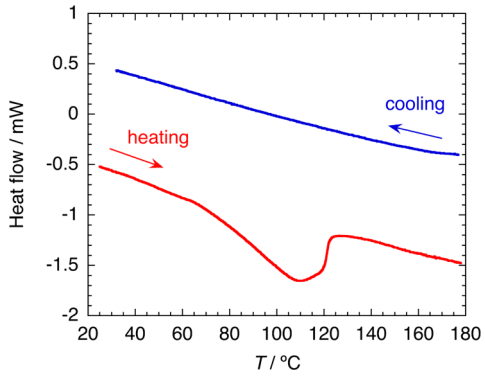

Figure 2. Differential scanning calorimetry chart for compound **1**. The sample was heated from room temperature to 180 °C at a rate of 2 °C min^{-1} under N_2 atmosphere and cooled at the same rate. The red and blue lines represent the heating and cooling processes, respectively.

DSC results for **1**. The samples were heated from room temperature to 180 °C and then cooled (heating and cooling rate = 2 °C min^{-1}). The benzene molecules (2.5 molecules per unit) were eliminated at 70−120 °C, giving an endothermic peak and a total enthalpy change of ΔH = −103.4 kJ mol^{-1}. It should be noted that this thermal change included a contribution from the structural change that occurred either during or after the elimination of the crystallization solvent (vide infra). There was no process to characterize the structural change that occurred during the cooling process (the blue line); therefore, we can conclude that **1′** was stable even at room temperature, giving good crystals without cracks. The structure of the desolvated **1′** was determined by single-crystal X-ray crystallography, as is described below. X-ray powder diffraction analysis confirmed that the other doped compounds were isostructural with **1′** (Figure S3, Supporting Information). It should be noted, however, that the transformation was reversible. When the dried sample was stored with benzene vapor, in a N_2 atmosphere, for 1 h, the compound completely returned to the solvated form (i.e., **1**), and this was confirmed from the XRPD patterns (Figure 3a) and the magnetic data

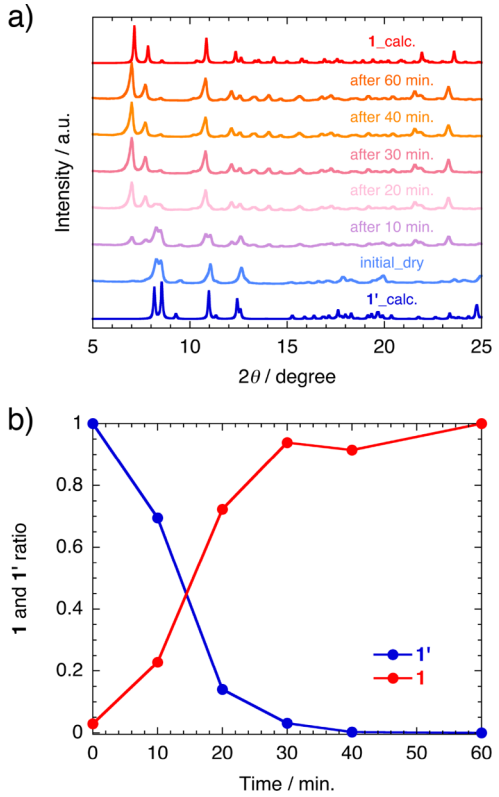

Figure 3. Variations in the X-ray powder diffraction (XRPD) spectra of **1′** in benzene atmosphere, measured every 10 min. (a) XRPD patterns and (b) time-dependency of the (010) index diffraction for **1′** (in blue) and of the (011) index diffraction for **1** (in red).

(Figure S4, Supporting Information). XRPD spectra of the powder samples in benzene atmosphere were collected every 10 min for 1 h (Figure 3b). The crystals did not pass through a new phase with a different lattice from **1′** and **1**, and the intermediate phase that had already appeared after 10 min was found to be simply a mixture of phases of **1′** and **1**, indicating that the benzene molecules were absorbed relatively quickly compared with their loss in the elimination process. The pattern for **1** was completely recovered after only 30 min, although the absorption speed was somewhat dependent on the sizes of the crystals.

Compound **1′** crystallized in the same space group (triclinic $P\bar{1}$) as compound **1**; however, only one kind of $[Ru_2]$ unit, with one BTDA-TCNQ and an inversion center, was characterized as being an asymmetric unit (Z = 1) (Figure 1b, d, and f). A chain feature similar to that in **1** was maintained in **1′**. The average Ru−O_{eq} length was 2.027 Å (Table S1, Supporting Information), indicating that the Ru oxidation state was $[Ru_2^{II,III}]^{+}$.[2,22] The charge on the BTDA-TCNQ moiety was

dx.doi.org/10.1021/ic500413j | Inorg. Chem. 2014, 53, 4716−4723

ρ = −0.97, as calculated from the Kistenmacher relationship (Table S2, Supporting Information),[2,23] which preserved the ionic form of **1**′. To compare the crystal packing between **1** and **1**′, it is convenient to transform the original unit cell of **1**′ to a' = $-\boldsymbol{a}$, b' = $\boldsymbol{b}$ + $\boldsymbol{c}$, and c' = $\boldsymbol{b}$ − $\boldsymbol{c}$ (Figure 1d and f), where $\boldsymbol{a}$, $\boldsymbol{b}$, and $\boldsymbol{c}$ are the original cell vectors for **1**′.[24] The chains in **1**′ were on the (011) plane of the modified cell, and the chain arrangement had an antiphase manner and was very similar to the arrangement in **1**. The $\pi-\pi$ stack between the 2-MeO-4-Cl-Ph group of [Ru_2] and BTDA-TCNQ was 3.491 Å ($d_{LS\text{-}p-p}$), the interchain [Ru_2]···BTDA-TCNQ distance was 7.55(1) Å, and the distances between the [Ru_2]s and between the BTDA-TCNQs were 10.54(1) Å (Figure S1, Supporting Information). Therefore, the packing feature of this chain layer, as well as many of the local structural dimensions of each chain, was preserved in **1**′. In fact, the a' (= 10.544 Å) and $-b'$ + c' (= 21.54 Å) vectors forming the (011) plane (corresponding to the chain layer) of **1**′ were very similar to the a (= 10.479 Å) and $-b$ + c (= 22.670 Å) vectors for **1**. This could be determined because the interstitial solvents were not in this layer but were between the chain layers in **1** (Figure 1c). Removing the interstitial solvents (2.5 molecules of benzene per unit) caused the [Ru_2]···[Ru_2] distance (or the distance between BTDA-TCNQs) in the ⟨011⟩ direction (i.e., the chain layer stacking direction) to change to 10.858(9) Å (Figure 1d), making the length ∼1.6 Å shorter than that in **1** (Figure S1, Supporting Information). The $\pi-\pi$ stack was still present, with $d_{LS\text{-}p-p}$ = 3.397 Å (Figure 1d) and a minimum C···C distance of 3.56(1) Å, and the interactions were stronger in **1**′ rather than in **1**.

Magnetic Properties of 1 and 1′. The magnetic properties of **1** and **1**′ were investigated over the temperature range 1.8−300 K (χT vs T plots for **1** and **1**′ are shown in Figure 4a and c, respectively). The χT of **1** slightly decreased from 1.68 cm^3 K mol^{-1} at 300 K to 1.66 cm^3 K mol^{-1} at 241 K (Figure 4a, inset) as the temperature decreased, then gradually increased, reaching a maximum of 3.36 cm^3 K mol^{-1} at 32 K, and then decreased sharply to 0.28 cm^3 K mol^{-1} at 1.8 K. This clearly indicates the ferrimagnetic spin arrangement S = 3/2 for $[Ru_2^{II,III}]^+$ and S = 1/2 for BTDA-$TCNQ^{\bullet-}$ occurred along the chain, even though the large anisotropy of the $[Ru_2^{II,II}]$ or $[Ru_2^{II,III}]^+$ unit would often have made it difficult to accurately evaluate the magnetic nature of such an assembled system.[11,25] Using the same method as was used to evaluate the N−I transition chain compound [Ru_2(2,3,5,6-F_4PhCO_2)$_4$(DMDCNQI)]·2(*p*-xylene) (2,3,5,6-$F_4PhCO_2^-$ = 2,3,5,6-tetrafluorobenzoate; DMDCNQI = 2,5-dimethyl-*N*,*N*′-dicyanoquinonediimine),[2] the data were simulated in the temperature range 120−300 K using an alternating chain model, with S_i = 3/2 and S_{i+1} = 1/2 in the Hamiltonian H = $-2J\sum_{i=1}^{N}\vec{S}_i\cdot\vec{S}_{i+1}$,[26] and an adequate parameter set was obtained; g_{Ru} = 2.08, g_{Rad} = 2.0 (fix), and J/k_B = −100.5 K. The exchange between $[Ru_2^{II,III}]^+$ and BTDA-$TCNQ^{\bullet-}$ was strongly antiferromagnetic, and this result agreed well with data found for the spin set $[Ru_2^{II,III}]^+$ and $DMDCNQI^{\bullet-}$ (the I phase in the N−I transition compound).[2] Indeed, except for the N−I transition compound,[2] this is the first time an assembled compound made up of $[Ru_2^{II,III}]^+$ and organic radical units has been isolated in a crystal form that allows its magneto-structural correlations to be defined. The strong antiferromagnetic coupling would have been caused by a large overlap between a frontier π^* orbital of $[Ru_2^{II,III}]^+$ and the π^* SOMO of BTDA-$TCNQ^{\bullet-}$.[9] While there was ferrimagnetic ordering at T_c = 6.2 K when the I phase of the N−I transition chain compound [Ru_2(2,3,5,6-F_4PhCO_2)$_4$(DMDCNQI)]·2(*p*-xylene) was present,[2] **1** exhibited antiferromagnetic long-range order at T_N = 10.9 K, suggesting that stronger interchain antiferromagnetic interactions were present in **1**. This was confirmed in the AC susceptibility data measured at zero DC field, in which only in-phase χ' susceptibility showed a peak at T_N (Figure S3, Supporting Information). Indeed, field-cooled magnetization curves measured when several DC fields were applied (Figure 5) and the field-dependence of the magnetization ($M-H$) curves measured at several temperatures (Figure 6a) showed that spin−flip phenomena occurred, and this finally allowed us to draw a phase diagram including the paramagnetic and antiferromagnetic phases (Figure 7). Using the mean-field approximation around an effective spin S_{eff} = $S_{[Ru2]}$ − S_{Rad} = 1, the interchain interaction was found to be zJ'_1/k_B = −0.74 K,

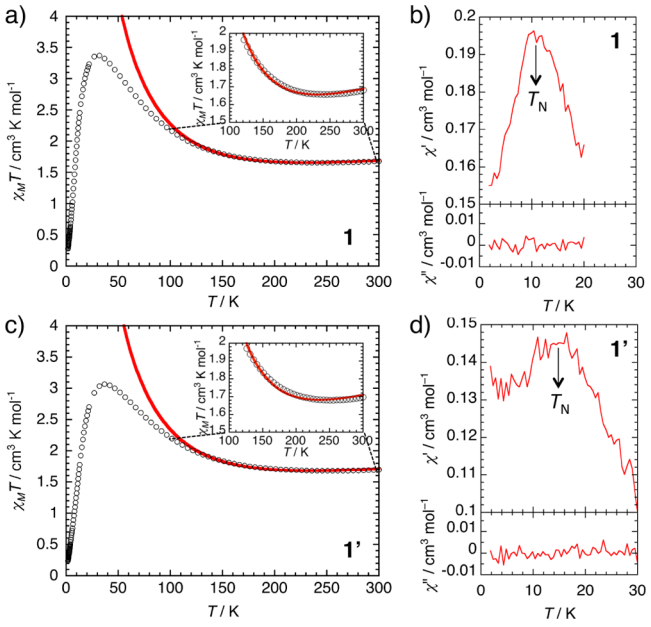

Figure 4. (a and c) Temperature dependence of χT and (b and d) AC susceptibilities for **1** and **1**′. DC data were measured when a DC field of 1 kOe was applied, and AC data were measured at 1 Hz under zero DC field and 3 Oe oscillating field. The insets in a and c are close-up views for the range 100−300 K. The solid red lines in a and c are the best-fit lines for the data in the temperature range 120−300 K; see text.

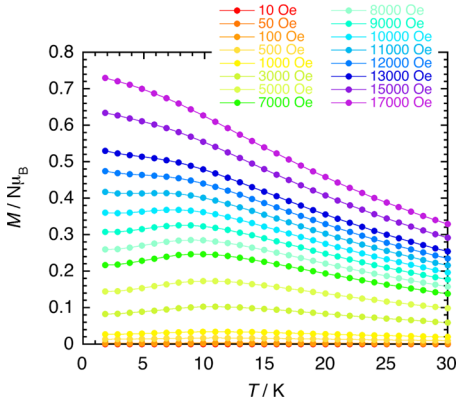

Figure 5. Field-cooled magnetization plots for **1**, measured at a range of fields.

dx.doi.org/10.1021/ic500413j | Inorg. Chem. 2014, 53, 4716−4723

based on the equation $2|zJ'|S_{eff}^2 \approx gS_{eff}\mu_B H_{ex}$, with the spin-flipping field H_{ex} = 1.10 T at 1.8 K and g = 2 (Figure 6b),[27] although zJ' was only useful for comparative purposes (vide infra).

The magnetic behavior of **1′** was basically similar to that of **1**. Indeed, the simulation of the χT data for **1′** (Figure 4c) gave the parameter set g_{Ru} = 2.09, g_{Rad} = 2.0 (fix), and J/k_B = −101.7 K, which is identical to the set for **1**. This supports the conclusion drawn from the structural analysis that the chain feature of **1** was preserved even in **1′**. However, the magnetic behavior of **1′** at low temperatures strongly reflected the packing difference between **1** and **1′**. The main difference was in the interchain distance in the ⟨011⟩ direction between the chain layers (11.849(3) between the BTDA-TCNQs and 12.467(2) Å for $[Ru(1)_2]\cdots[Ru(2)_2]$ for **1** but 10.858(9) Å for both distances for **1′**; vide supra). Consequently, T_N for **1′** was shifted to a higher temperature, 14 K. The zJ' was estimated to be zJ'_1/k_B = −1.21 K from the spin-flip field (H_{ex} = 1.80 T at 1.8 K), which was larger than the value for **1**, and this was attributed to the shorter interchain distance.[27]

Variations in the Antiferromagnetic Phases of the Doped Compounds. The χT vs T data in the temperature range 120−300 K were simulated for the doped compounds using the alternating chain model; this simulation accounted for the effective spins $S_{[Ru2]}' = 3/2(1-x)$ and $S_{Rad}' = 1/2(1-x)$ (Figure S6, Supporting Information). The magnitude of the exchange parameter J between $[Ru_2^{II,III}]^+$ and BTDA-TCNQ$^{\bullet-}$ was basically identical to that for **1**, with $J \approx -100$ K (Table S3, Supporting Information). The doping of $[Rh_2^{II,II}]$ species into the ionic chain enabled a mixed valence set A^-A^0 to be formed in a chain domain between $[Rh_2^{II,II}]$ species.[12] Nevertheless, the results indicated that the effect of the mixed valence set in the doped compounds was not dominated by the magnetic correlation, although the $[Rh_2^{II,II}]$ dopants acted as defects, affecting the effective magnetic domain length. The doped compounds, except for **Rh-16%** and **Rh-16%′**, each underwent an antiferromagnetic phase transition similar to that for **1** and **1′**, and this can easily be seen in the M−H curves at low fields (Figure 6b). The T_N was 5.9 K for **Rh-3%**, 3.7 K for **Rh-5%**, and 9.9 and 9.2 K, respectively, for the solvent-free compounds **Rh-3%′** and **Rh-5%′** (Figure 7a). Interestingly, these T_Ns were approximately inversely proportional to the amount of dopant present (Figure 7b), although the magnitude of the intrachain exchange coupling between the composite spins remained unchanged (therefore, the transition for **Rh-16%** and **Rh-16%′** was no longer detectable at temperatures above 1.8 K). In addition, considering the isostructural features of the fresh and dried compound series, the interchain distances should be constant in each series, independent of the amount doped. The simple model based on the individual local spins S = 3/2 and S = 1/2 could, therefore, no longer be used alone to explain the doping-dependent T_N. The spins were changed to the effective spins, i.e., $S_{[Ru2]}' = 3/2(1-x)$ and $S_{Rad}' = 1/2(1-x)$ for the doped system, and these spin values were very useful for evaluating the nature of the magnetic short-range domains in the chain. This was because the mean size of the one-dimensional (*1-D*) domains, which will be proportional to the effective spin $S_{eff}' = (S_{[Ru]}' - S_{Rad}') = (1-x)$, will be a crucial factor in determining T_N when the interchain dipole−dipole interactions play an important role in the formation of *3-D* domains. The dipole energy is proportional to the magnetic moment $\mu = g\mu_B S_{eff}'$ and the inverse of r^3 (i.e., $1/r^3$) because r is the vector distance between S_{eff}' spins.[27] In fact, H_{ex} is also

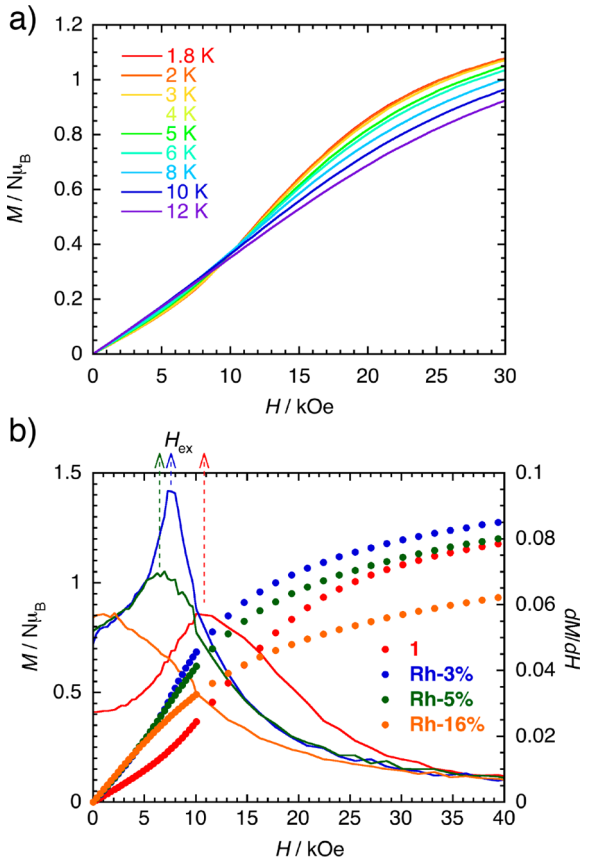

Figure 6. (a) Field dependence of the magnetization (M−H plots) for **1**, measured at a range of temperatures, and (b) M−H plots and dM/dH plots for **1**, **Rh-3%**, **Rh-5%**, and **Rh-16%** (as-synthesized samples).

approximately proportional to the effective spin $S_{eff}' = (1-x)$, and zJ' estimated using S_{eff}' were $zJ'_{Rh\text{-}3\%}/k_B$ = −0.53 K (H_{ex} = 0.77 T) and $zJ'_{Rh\text{-}5\%}/k_B$ = −0.45 K (H_{ex} = 0.64 T) for **Rh-3%** and **Rh-5%**, respectively, and $zJ'_{Rh\text{-}3\%'}/k_B$ = −1.16 K (H_{ex} = 1.67 T) and $zJ'_{Rh\text{-}5\%'}/k_B$ = −1.24 K (H_{ex} = 1.76 T) for **Rh-3%′** and **Rh-5%′**, respectively, which were in the same range as zJ'_1 and $zJ'_{1'}$, respectively. This proves that T_N is closely associated with the *1-D* domain defined by S_{eff}'.

CONCLUSIONS

Dipole−dipole interactions between *1-D* short-range domains are key to the magnetic ordering processes in anisotropic low-dimensional compounds, such as the series presented here, and doping diamagnetic species into the magnetic chain, systematically decreasing the magnetic correlation in the chain, was successfully shown to change the T_N. This allows the mean size of magnetic domains, which is proportional to $S_{eff}' = (1-x)$, to be tuned. Modifying the interchain distance through a crystal-to-crystal transformation allows the T_N to be modified: this directly tunes the vector distance r between the interchain magnetic domains, which is inversely proportional to the dipole−dipole interactions. Combining these two methods, chemical modification (i.e., doping) and crystal-to-crystal transformation, allows the magnetic ordering to be systematically tuned. Such a systematic investigation into magnetic ordering mechanisms in a low-dimensional system is without precedent. A good understanding of the nature of magnetic ordering in such a low-dimensional anisotropic system, which involves both strong and weak correlations, is extremely

dx.doi.org/10.1021/ic500413j | Inorg. Chem. 2014, 53, 4716−4723

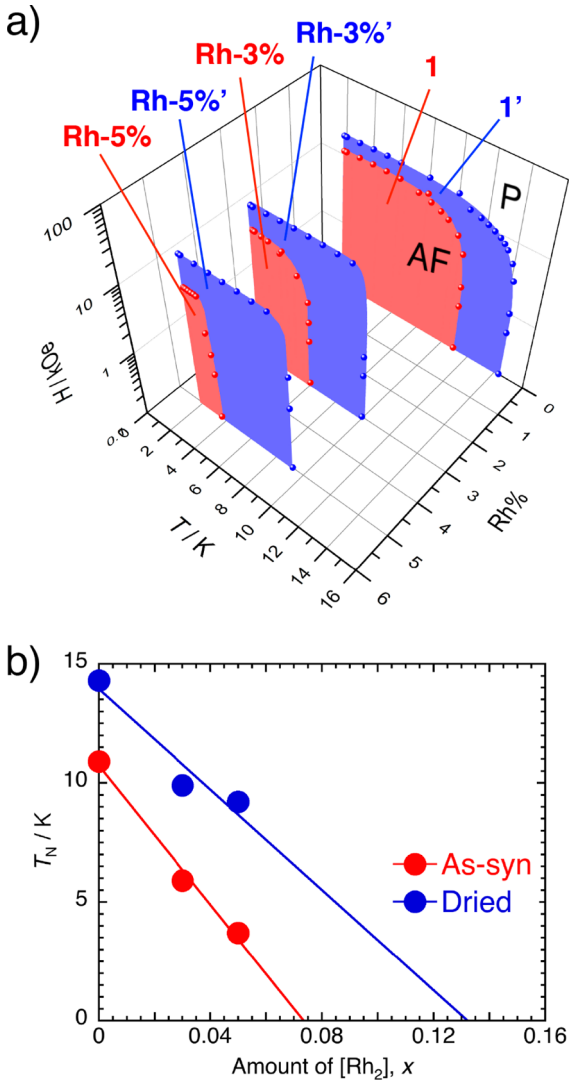

Figure 7. (a) $H-T$ phase diagrams for the as-synthesized samples **1**, **Rh-3%**, and **Rh-5%**, and the dried samples **1′**, **Rh-3%′**, and **Rh-5%′**. (b) Variation of T_N as a function of the amount of [Rh_2] dopant present, x (the solid lines are the least-squared fitted lines).

important for designing molecule-based magnetic and electronic materials; it may be possible to discover a new phase, as the slow relaxation of magnetization-like single-chain magnet behavior was found in an antiferromagnetic phase.[28]

■ ASSOCIATED CONTENT

Ⓢ Supporting Information

CIF format X-ray crystallographic data for **1′**; the comparison of structures among **1**, the doped compounds, and **1′**; magnetic parameters; packing diagrams of **1** and **1′**; TGA plots; XRPD patterns of the dried compounds; and χT vs T plots for the doped compounds and their dried compounds. This material is available free of charge via the Internet at http://pubs.acs.org.

■ AUTHOR INFORMATION

Corresponding Author

*Tel: +81-22-215-2030. Fax: +81-22-215-2031. E-mail: miyasaka@imr.tohoku.ac.jp.

Notes

The authors declare no competing financial interest.

■ ACKNOWLEDGMENTS

We thank Mr. Yuichiro Asai (Department of Chemistry, Tohoku University) for his help in synthesizing the compounds. This work was supported by a Grant-in-Aid for Scientific Research (No. 21350032; 24245012) and for Innovative Areas ("Coordination Programming" Area 2107, No. 24108714) from the Ministry of Education, Culture, Sports, Science, and Technology, Japan, The Sumitomo Foundation, and The Asahi Glass Foundation.

■ REFERENCES

(1) (a) Miller, J. S.; Epstein, A. J. *Angew. Chem., Int. Ed. Engl.* **1994**, *33*, 385−415. (b) Miller, J. S. *Chem. Soc. Rev.* **2011**, *40*, 3266−3296.

(2) Miyasaka, H.; Motokawa, N.; Chiyo, T.; Takemura, M.; Yamashita, M.; Sagayama, H.; Arima, T. *J. Am. Chem. Soc.* **2011**, *133*, 5338−5345.

(3) (a) Summerville, D. A.; Cape, T. W.; Johnson, E. D.; Basolo, F. *Inorg. Chem.* **1978**, *17*, 3297−3300. (b) Miller, J. S.; Calabrese, J. C.; McLean, R. S.; Epstein, A. J. *Adv. Mater.* **1992**, *4*, 498−501. (c) Zhou, P.; Morin, B. G.; Epstein, A. J.; McLean, R. S.; Miller, J. S. *J. Appl. Phys.* **1993**, *73*, 6569−6571. (d) Miller, J. S.; Vazquez, C.; Calabrese, J. C.; McLean, R. S.; Epstein, A. J. *Adv. Mater.* **1994**, *3*, 217−221. (e) Miller, J. S.; Vazquez, C.; Jones, N. L.; McLean, R. S.; Epstein, A. J. *J. Mater. Chem.* **1995**, *5*, 707−711. (f) Brinckerhoff, W. B.; Morin, B. G.; Brandon, E. J.; Miller, J. S.; Epstein, A. J. *J. Appl. Phys.* **1996**, *79*, 6147−6149. (g) Böhm, A.; Vazquez, C.; Mclean, R. S.; Calabrese, J. C.; Kalm, S. E.; Manson, J. L.; Epstein, A. J.; Miller, J. S. *Inorg. Chem.* **1996**, *35*, 3083−3088. (h) Miller, J. S.; Epstein, A. J. *Chem. Commun.* **1998**, 1319−1325. (i) Brandon, E. J.; Kollmar, C.; Miller, J. S. *J. Am. Chem. Soc.* **1998**, *120*, 1822−1826. (j) Brandon, E. J.; Rittenberg, D. K.; Arif, A. M.; Miller, J. S. *Inorg. Chem.* **1998**, *37*, 3376−3384. (k) Brandon, E. J.; Arif, A. M.; Burkhart, B. M.; Miller, J. S. *Inorg. Chem.* **1998**, *37*, 2792−2798. (l) Rittenberg, D. K.; Miller, J. S. *Inorg. Chem.* **1999**, *38*, 4838−4848. (m) Rittenberg, D. K.; Sugiura, K.; Sakata, Y.; Guzei, I. A.; Rheingold, A. L.; Miller, J. S. *Chem.—Eur. J.* **1999**, *5*, 1874−1881. (n) Rittenberg, D. K.; Baars-Hibbe, L.; Böhm, A.; Miller, J. S. *J. Mater. Chem.* **2000**, *10*, 241−244. (o) Miller, J. S. *Inorg. Chem.* **2000**, *39*, 4392−4408.

(4) (a) Sugiura, K.; Mikami, S.; Johnson, M. T.; Miller, J. S.; Iwasaki, K.; Umishita, K.; Hino, S.; Sakata, Y. *J. Mater. Chem.* **2000**, *10*, 959−964. (b) Johnson, M. T.; Arif, A. M.; Miller, J. S. *Eur. J. Inorg. Chem.* **2000**, *6*, 1781−1787.

(5) (a) Wynn, C. M.; Gîrtu, M. A.; Brinckhoff, W. B.; Sugiura, K.-I.; Miller, J. S.; Epstein, A. J. *Chem. Mater.* **1997**, *9*, 2156−2163. (b) Wynn, C. M.; Gîrtu, M. A.; Miller, J. S.; Epstein, A. J. *Phys. Rev. B* **1997**, *56*, 315−320. (c) Wynn, C. M.; Gîrtu, M. A.; Miller, J. S.; Epstein, A. J. *Phys. Rev. B* **1997**, *56*, 14050−14057.

(6) Brandon, E. J.; Rogers, R. D.; Burkhart, B. M.; Miller, J. S. *Chem.—Eur. J.* **1998**, *4*, 1938−1943.

(7) Sugiura, K.; Mikami, S.; Johnson, M. T.; Raebiger, J. W.; Miller, J. S.; Iwasaki, K.; Okada, Y.; Hino, S.; Sakata, Y. *J. Mater. Chem.* **2001**, *11*, 2152−2158.

(8) Miyasaka, H.; Madanbashi, T.; Sugimoto, K.; Nakazawa, Y.; Wernsdorfer, W.; Sugiura, K.; Yamashita, M.; Coulon, C.; Clérac, R. *Chem.—Eur. J.* **2006**, *12*, 7028−7040.

(9) Miyasaka, H. *Acc. Chem. Res.* **2013**, *46*, 248−257.

(10) Cotton, F. A.; Walton, R. A. *Multiple Bonds between Metal Atoms*, 2nd ed.; Oxford University Press: Oxford, U.K., 1993.

(11) (a) Miyasaka, H.; Campos-Fernández, C. S.; Clérac, R.; Dunbar, K. R. *Angew. Chem., Int. Ed.* **2000**, *39*, 3831−3835. (b) Miyasaka, H.; Izawa, T.; Takahashi, N.; Yamashita, M.; Dunbar, K. R. *J. Am. Chem. Soc.* **2006**, *128*, 11358−11359. (c) Motokawa, N.; Oyama, T.; Matsunaga, S.; Miyasaka, H.; Sugimoto, K.; Yamashita, M.; Lopez, N.; Dunbar, K. R. *Dalton Trans.* **2008**, 4099−4102. (d) Motokawa, N.; Miyasaka, H.; Yamashita, M.; Dunbar, K. R. *Angew. Chem., Int. Ed.* **2008**, *47*, 7760−7763. (e) Motokawa, N.; Oyama, T.; Matsunaga, S.; Miyasaka, H.; Yamashita, M.; Dunbar, K. R. *CrystEngComm* **2009**, *11*,

2121−2130. (f) Miyasaka, H.; Motokawa, N.; Matsunaga, S.; Yamashita, M.; Sugimoto, K.; Mori, T.; Toyota, N.; Dunbar, K. R. *J. Am. Chem. Soc.* **2010**, *132*, 1532−1544. (g) Motokawa, N.; Matsunaga, S.; Takaishi, S.; Miyasaka, H.; Yamashita, M.; Dunbar, K. R. *J. Am. Chem. Soc.* **2010**, *132*, 11943−11951. (h) Miyasaka, H.; Morita, T.; Yamashita, M. *Chem. Commun.* **2011**, *47*, 271−273. (i) Nakabayashi, K.; Nishio, M.; Kubo, K.; Kosaka, W.; Miyasaka, H. *Dalton Trans.* **2012**, *41*, 6072−6074.

(12) Nishio, M.; Hoshino, N.; Kosaka, W.; Akutagawa, T.; Miyasaka, H. *J. Am. Chem. Soc.* **2013**, *135*, 17715−17718.

(13) (a) Larionova, J.; Chavan, S. A.; Yakhmi, J. V.; Frøystein, A. G.; Sletten, J.; Sourisseau, C.; Kahn, O. *Inorg. Chem.* **1997**, *36*, 6374−6381. (b) Maspoch, D.; Ruiz-Molina, D.; Wurst, K.; Domingo, N.; Cavallini, M.; Biscarini, F.; Tejada, J.; Rovira, C.; Veciana, J. *Nat. Mater.* **2003**, *2*, 190−195. (c) Kurmoo, M.; Kumagai, H.; Hughes, S. M.; Kepert, C. J. *Inorg. Chem.* **2003**, *42*, 6709−6722. (d) Kurmoo, M.; Kumagai, H.; Chapman, K. W.; Kepert, C. J. *Chem. Commun.* **2005**, 3012−3014. (e) Yanai, N.; Kaneko, W.; Yoneda, K.; Ohba, M.; Kitagawa, S. *J. Am. Chem. Soc.* **2007**, *129*, 3496−3497. (f) Milon, J.; Daniel, M.-C.; Kaiba, A.; Guionneau, P.; Brandès, S.; Sutter, J.-P. *J. Am. Chem. Soc.* **2007**, *129*, 13872−13878. (g) Lopez, N.; Zhao, H.; Prosvirin, A. V.; Chouai, A.; Shatruk, M.; Dunbar, K. R. *Chem. Commun.* **2007**, 4611−4613. (h) Cheng, X.-N.; Zhang, W.-X.; Chen, X.-M. *J. Am. Chem. Soc.* **2007**, *129*, 15738−15739. (i) Ohkoshi, S.; Tsunobuchi, Y.; Takahashi, H.; Hozumi, T.; Shiro, M.; Hashimoto, K. *J. Am. Chem. Soc.* **2007**, *129*, 3084−3085. (j) Ghosh, S. K.; Kaneko, W.; Kiriya, D.; Ohba, M.; Kitagawa, S. *Angew. Chem., Int. Ed.* **2008**, *47*, 8843−8847. (k) Zhang, Y.-J.; Liu, T.; Kanegawa, S.; Sato, O. *J. Am. Chem. Soc.* **2009**, *131*, 7942−7943. (l) Duan, Z.; Zhang, Y.; Zhang, B.; Zhu, D. *J. Am. Chem. Soc.* **2009**, *131*, 6934−6935. (m) Zhang, W.-X.; Xue, W.; Chen, X.-M. *Inorg. Chem.* **2011**, *50*, 309−316. (n) Wriedt, M.; Yakovenko, A. A.; Halder, G. J.; Prosvirin, A. V.; Dunbar, K. R. *J. Am. Chem. Soc.* **2013**, *135*, 4040−4050.

(14) Boudreaux, E. A.; Mulay, L. N. *Theory and Applications of Molecular Paramagnetism*; John Wiley & Sons: New York, 1976.

(15) Cromer, D. T.; T. Waber, J. *International Tables for Crystallography*; The Kynoch Press: Birmingham, England, 1974; Vol *IV*, Table 2.2A.

(16) Ibers, J. A.; Hamilton, W. C. *Acta Crystallogr.* **1964**, *17*, 781−782.

(17) Creagh, D. C.; McAuley, W. J. *International Tables for Crystallography*; Wilson, A. J. C., Ed.; Kluwer Academic Publishers: Boston, MA, 1992; Vol *C*, pp 219−222, Table 4.2.6.8.

(18) Creagh, D. C.; Hubbell, J. H. *International Tables for Crystallography*; Wilson, A. J. C., Ed.; Kluwer Academic Publishers: Boston, MA, 1992; Vol *C*, pp 200−206, Table 4.2.4.3.

(19) *CrystalStructure 4.0.1: Crystal Structure Analysis Package*, Rigaku Corporation: Tokyo, 2000−2010.

(20) Sheldrick, G. M. *Acta Crystallogr., Sect. A* **2008**, *64*, 112−122.

(21) (a) Ouyang, X.; Campana, C.; Dunbar, K. R. *Inorg. Chem.* **1996**, *35*, 7188−7189. (b) Miyasaka, H.; Campos-Fernández, C. S.; Galán-Mascarós, J. R.; Dunbar, K. R. *Inorg. Chem.* **2000**, *39*, 5870−5873.

(22) Miyasaka, H.; Motokawa, N.; Atsuumi, R.; Kamo, H.; Asai, Y.; Yamashita, M. *Dalton Trans.* **2011**, *40*, 673−682.

(23) Kistenmacher, T. J.; Emge, T. J.; Bloch, A. N.; Cowan, D. O. *Acta Crystallogr., Sect. B* **1982**, *38*, 1193−1199.

(24) The unit cell parameters for **1**′ were transformed into a' = 10.544(11) Å, b' = 12.330(10) Å, c' = 18.958(15) Å, a' = 94.89(3)°, b' = 91.23(6)°, g' = 82.66(9)°, V' = 2435(4) Å3, and Z' = 2, where $a' = -\boldsymbol{a}$, $b' = \boldsymbol{b} + \boldsymbol{c}$, $c' = \boldsymbol{b} - \boldsymbol{c}$ ($\boldsymbol{a}$, $\boldsymbol{b}$, and $\boldsymbol{c}$ are the original cell vectors for **1**′).

(25) (a) Aquino, M. A. S. *Coord. Chem. Rev.* **1998**, *170*, 141−202. (b) Aquino, M. A. S. *Coord. Chem. Rev.* **2004**, *248*, 1025−1045. (c) Mikuriya, M.; Yoshioka, D.; Handa, M. *Coord. Chem. Rev.* **2006**, *250*, 2194−2211.

(26) Drillon, M.; Coronado, E.; Beltrain, D.; Georges, R. *Chem. Phys.* **1983**, *79*, 449−453.

(27) Carlin, R. L. *Magnetochemistry*; Springer-Verlag: Berlin, 1986.

(28) (a) Coulon, C.; Clérac, R.; Wernsdorfer, W.; Colin, T.; Miyasaka, H. *Phys. Rev. Lett.* **2009**, *102*, 167204−1−4. (b) Miyasaka, H.; Takayama, K.; Saitoh, A.; Furukawa, S.; Yamashita, M.; Clérac, R. *Chem.—Eur. J.* **2010**, *16*, 3656−3662.